





Tuning interchain ferromagnetic instability in $A_2Cr_3As_3$ ternary arsenides by chemical pressure and uniaxial strain

Giuseppe Cuono ^{1,*} Filomena Forte,^{2,3} Alfonso Romano,^{3,2} Xing Ming ⁴ Jianlin Luo,^{5,6,7} Carmine Autieri ^{1,2,†} and Canio Noce ^{3,2}

¹*International Research Centre Magtop, Institute of Physics, Polish Academy of Sciences, Aleja Lotników 32/46, PL-02668 Warsaw, Poland*

²*Consiglio Nazionale delle Ricerche CNR-SPIN, UOS Salerno, I-84084 Fisciano (Salerno), Italy*

³*Dipartimento di Fisica “E.R. Caianiello,” Università degli Studi di Salerno, I-84084 Fisciano (SA), Italy*

⁴*College of Science, Guilin University of Technology, Guilin 541004, People’s Republic of China*

⁵*Beijing National Laboratory for Condensed Matter Physics and Institute of Physics, Chinese Academy of Sciences, Beijing 100190, China*

⁶*Songshan Lake Materials Laboratory, Dongguan, Guangdong 523808, China*

⁷*School of Physical Sciences, University of Chinese Academy of Sciences, Beijing 100190, China*



(Received 8 August 2020; revised 23 December 2020; accepted 20 May 2021; published 2 June 2021)

We analyze the effects of chemical pressure induced by alkali-metal substitution and uniaxial strain on magnetism in the $A_2Cr_3As_3$ ($A=Na, K, Rb, \text{ and } Cs$) family of ternary arsenides with quasi-one-dimensional structure. Within the framework of the density functional theory, we predict that the nonmagnetic phase is very close to a three-dimensional collinear ferrimagnetic state, which realizes in the regime of moderate correlations, such tendency being common to all the members of the family with very small variations due to the different interchain ferromagnetic coupling. We uncover that the stability of such interchain ferromagnetic coupling has a nonmonotonic behavior with increasing the cation size, being critically related to the degree of structural distortions which is parametrized by the Cr-As-Cr bonding angles along the chain direction. In particular, we demonstrate that it is boosted in the case of the Rb, in agreement with recent experiments. We also show that uniaxial strain is a viable tool to tune the nonmagnetic phase towards an interchain ferromagnetic instability. The modification of the shape of the Cr triangles within the unit cell favors the formation of a net magnetization within the chain and of a ferromagnetic coupling among the chains. This study can provide relevant insights about the interplay between superconductivity and magnetism in this class of materials.

DOI: [10.1103/PhysRevMaterials.5.064402](https://doi.org/10.1103/PhysRevMaterials.5.064402)

I. INTRODUCTION

In recent years, a great deal of attention has been devoted to the competing quantum orders which develop in transition metal pnictides. In this context, one of the most relevant examples is represented by the recently discovered Cr-based arsenide family $A_2Cr_3As_3$ ($A=Na, K, Rb, \text{ and } Cs$) [1–4]. This series has been shown to represent an ideal platform for the study of the interplay between magnetism and structural instabilities [5–9], as well as of other relevant features such as noncentrosymmetry and quasi-one-dimensional properties [10,11].

The crystal structure of the above-mentioned compounds, reported in Fig. 1, features Cr_3As_3 chains forming double-wall subnanotubes (DWSN), where the inner-wall tubes are constructed by Cr triangles and the outer-wall tubes by As triangles, separated by columns of A^+ ions [1–4]. Band structure calculations indicate that the states governing the electronic physics at the Fermi energy E_F are mainly Cr $3d$ orbitals [12–14].

Interestingly, in these compounds a superconducting phase [15–17] also emerges at ambient pressure, which is so far unique for systems containing chromium [7,18–26]. Notably, superconductivity occurs with a background of ferromagnetic (FM) spin fluctuations [27], which is quite rare and make a major difference with respect to cuprates, iron-based and heavy-fermion systems where unconventional superconductivity occurs close to an antiferromagnetic (AFM) instability [28].

Recent NMR measurements reveal the evidence of strong spin fluctuations. In the Rb-based compound, strong enhancement of the spin susceptibility suggests that three-dimensional (3D) FM fluctuations are present near T_c [29]. Analogous experiments in $K_2Cr_3As_3$ show that Cr spin fluctuations may have a dominant antiferromagnetic character [15], while in $Na_2Cr_3As_3$ and $Cs_2Cr_3As_3$ they are suppressed [30]. Therefore, a systematic comparison of how alkali substitution modifies the FM fluctuations among the members of the family is needed in order to shed light on the magnetic ground states of these compounds, and possibly on the superconducting pairing mechanism. The latter still remains elusive, with conflicting hypotheses that have been suggested, ranging from spin fluctuations to conventional phonons [5,15–17,31–33].

Recently, structural distortions breaking the high-symmetry hexagonal structure have been experimentally

*gcuomo@magtop.ifpan.edu.pl

†autieri@magtop.ifpan.edu.pl

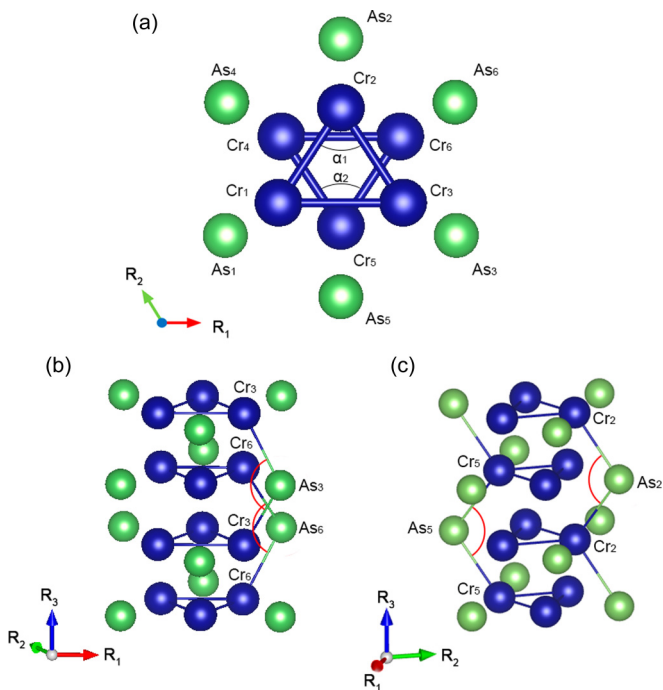


FIG. 1. (a) Cr triangles belonging to the $[(\text{Cr}_3\text{As}_3)^{2-}]_\infty$ subnanotubes of the $\text{A}_2\text{Cr}_3\text{As}_3$ compounds. The deviation from the ideal hexagonal structure is parametrized by the angles α_1 and α_2 . Blue and green circles denote Cr and As atoms, respectively. (b),(c) Cr-As-Cr bonding angles along different chain direction (see the reported axes).

detected in $\text{K}_2\text{Cr}_3\text{As}_3$ [6]. On this basis, we have demonstrated that there is a strong interplay between these distortions and the magnetic properties of that compound [34]. In particular, orthorhombic distortions make the Cr triangles in the DWSN no longer equilateral, which is detrimental to magnetic frustration, also changing the nature of the magnetic ground state. Indeed, without considering the distortions, the system shows a magnetic instability towards the all-in/all-out configuration [8]. On the contrary, the presence of distortions has been shown to promote a new kind of instability towards a collinear ferrimagnetic ground state with a net magnetization in the ab plane. Moreover, we have studied both compounds KCr_3As_3 and $\text{K}_2\text{Cr}_3\text{As}_3$ in a wide range of the Coulomb repulsion U , from $U = 0$ to 3 eV finding that, by taking into account the distortions, the experimental results are reproduced in a range of the Coulomb repulsion between 0.25 and 0.40 eV. Therefore, we can state that $\text{K}_2\text{Cr}_3\text{As}_3$ has a nonmagnetic ground state but is close to a collinear ferrimagnetic phase [34].

In this paper, we extend this systematic study to all the members of the $\text{A}_2\text{Cr}_3\text{As}_3$ family in the presence of structural distortions and show that the tendency towards an interchain FM instability may be tuned via chemical substitution or uniaxial strain. Isovalent doping can induce chemical pressure effects without introducing carriers. At the same time it alters the interchain hopping, also affecting the coupling between the chains. Moreover, it may cause slight modifications of the crystal structure along the chain, thus altering the intrachain spin correlations. On the other hand, uniaxial strain, e.g., the

modification of the lattice constant along a specific direction, is effective especially in one-dimensional (1D) compounds, since it allows one to continually modify the distances parallel or orthogonal to the chain direction, and thus can provide a pathway to explore the related phase diagram.

We perform a systematic study on the members of the $\text{A}_2\text{Cr}_3\text{As}_3$ family ($A=\text{Na}, \text{K}, \text{Rb}, \text{and Cs}$), showing that all the compounds are in the proximity of a collinear ferrimagnetic configuration within the chain, regardless of the A species. Our results also demonstrate that interchain ferromagnetic exchange is promoted in the regime of moderate on-site electronic correlation, and that the stability of such ferromagnetic coupling has a nonmonotonic behavior with the size of the cation. We single out the structural parameters that govern the formation of the ferromagnetic coupling, focusing in particular on the Cr-As-Cr bond angles originating from the alternate distribution of alkali-metal ions along the chain direction. Furthermore, we show that uniaxial strain affects the interchain FM instability by lowering the critical value of the local Coulomb repulsion above which the magnetic moments are stabilized.

The paper is organized as follows. In Sec. II we present the computational details of our approach. Section III is devoted to a systematic study of the magnetic configurations within the chain for all the compounds. In Sec. IV we analyze the effects of the interchain magnetic coupling on the stability of the FM configurations, together with the corresponding structural fingerprints. In Sec. V we consider the case of a compressive/tensile strain field applied along an in-plane direction, while in Sec. VI we discuss the electronic properties, i.e., the energy spectra and the orbitally resolved densities of states, for all the members of the $\text{A}_2\text{Cr}_3\text{As}_3$ family. Finally, Sec. VII is devoted to the conclusions.

II. COMPUTATIONAL DETAILS

We have performed density functional theory (DFT) calculations by using the VASP package [35–37] based on the plane wave basis set and the projector augmented wave [38] method with a cutoff of 440 eV for the plane wave basis. We have used the PBEsol exchange-correlation method [39], which provides an excellent functional for the atomic relaxation in solids. We need good accuracy for the structural properties, given the strong coupling between electronic and structural degrees of freedom in this class of materials. A $4 \times 4 \times 10$ k -point grid, which corresponds to 160 k points in the first Brillouin zone, has been employed for the calculations concerning the chains. In order to describe the electronic correlations associated with the Cr $3d$ states, a Coulomb repulsion U has been added to our functional [40]. We have used values of U ranging from 0 to 3 eV. The relevant region is until 1.5 eV, that is, for larger values of U we are in the saturation region. We have performed structural relaxation minimizing the internal atomic positions and forces to less than $0.01 \text{ eV}/\text{\AA}$. The volume calculated in DFT usually deviates from the experimental value by a few percent. While in most of the cases this deviation is negligible, it could play a relevant role in systems such as the one investigated here, characterized by a strong interplay between magnetic and structural properties. Though in other studies on Cr-based compounds a full lattice relaxation procedure has

TABLE I. Lattice constants of the compounds of the family $A_2Cr_3As_3$. The space group is the $P\bar{6}m2$ (No. 187).

$A_2Cr_3As_3$	$A = Na$ [1]	$A = K$ [2]	$A = Rb$ [3]	$A = Cs$ [4]
a (Å)	9.2390	9.9832	10.2810	10.6050
c (Å)	4.2090	4.2304	4.2421	4.2478

been adopted [8,12,41], we decided to perform the relaxation of the atomic positions having fixed the volume of the unit cell to its experimental value. In this way we exclude the possibility of volume variations which would affect the magnetic properties of the system. We have also checked that when the constraint on the volume is removed, our results coincide, for instance, with those obtained in Ref. [41].

The relaxation procedure started from equilateral triangles for both collinear and noncollinear magnetic configurations, also including the effect of the spin-orbit coupling. We found that once the structural relaxation converges, the energetically favored configuration is characterized by distorted Cr-ion triangles, with an arrangement of the magnetic moments which is always collinear. The lattice vectors of the unit cell are $\mathbf{R}_1 = (a, 0, 0)$, $\mathbf{R}_2 = (-a/2, \sqrt{3}a/2, 0)$, and $\mathbf{R}_3 = (0, 0, c)$. To calculate the interchain coupling we have doubled the unit cell along the \mathbf{R}_1 direction, and we have used a supercell with two formula units and a $2 \times 4 \times 10$ k -point grid.

III. CHAIN GROUND STATE IN THE $A_2Cr_3As_3$ FAMILY

The $A_2Cr_3As_3$ family is characterized by a markedly 1D structure, with Cr_3As_3 linear chains separated by A^+ ions sitting on different crystallographic sites [1–4]. In Fig. 1 we report the notation used for the inequivalent Cr and As atoms, together with the angles among the Cr atoms within the \mathbf{R}_1 - \mathbf{R}_2 plane and the Cr-As-Cr bonding angles along the chain. Increasing the atomic radius from Na^+ to K^+ , Rb^+ , and Cs^+ induces chemical pressure effects which lead to the expansion of the interchain distance by keeping the linear chain structure almost unchanged, as one can see from the data reported in Table I.

We note that the superconducting critical temperature T_c progressively increases in the series $A_2Cr_3As_3$ as the atomic number of the alkaline ion decreases. Actually, T_c is found to be ~ 2.2 K in $Cs_2Cr_3As_3$ [4], 4.8 K in $Rb_2Cr_3As_3$ [3], 6.1 K in $K_2Cr_3As_3$ [2], and 8.6 K in $Na_2Cr_3As_3$ [1]. This finding thus clearly indicates a systematic trend of the chemical pressure effect on the superconducting mechanism [1–4]. Of course, reducing the A -cation size, the unit-cell volume decreases too. However, it has been shown that the application of hydrostatic pressure on $K_2Cr_3As_3$, which differently from the chemical pressure reduces the volume isotropically, leads to a reduction of T_c [10,42,43]. This means that the two kinds of pressure have opposite effects on the superconducting transition.

From the structural point of view the chemical pressure may affect other relevant structural parameters, which are expected to play a role in the most favorable magnetic stable phases. We know from previous *ab initio* studies on $K_2Cr_3As_3$ [6,34] that localized orthorhombic distortions of the CrAs sublattice together with associated K displacements cause the

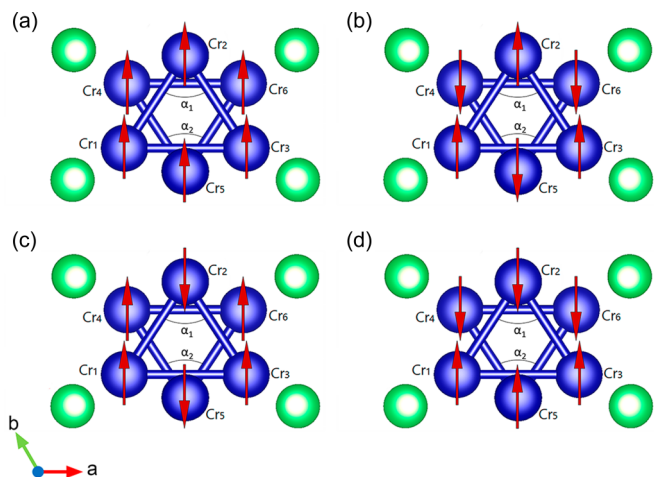


FIG. 2. Cr-spin configurations investigated in the paper, defined as (a) the ferromagnetic state (FM), (b) the interlayer antiferromagnetic state (AFM), (c) the up-up-down/up-up-down ($\uparrow\uparrow\downarrow - \uparrow\uparrow\downarrow$) stripe state, and (d) the up-up-down/down-down-up ($\uparrow\uparrow\downarrow - \downarrow\downarrow\uparrow$) zigzag state.

Cr triangles in the DWSN to be no longer equilateral. These deformations, described in terms of the angles α_1 and α_2 reported in Fig. 1, weaken magnetic frustration, favoring a collinear stripe phase within the chains [34]. The structural distortions explicitly taken into account in our approach make the two magnetic moments at the basis of each triangle different from the one at the vertex.

However, other parameters are worth paying attention to. The alternate distribution of the alkali-metal ions along the chain direction gives rise to different bond angles of Cr-As-Cr, as shown in Fig. 1(b). Due to the distorted Cr triangles, we can distinguish four independent angles, Cr_3 - As_3 - Cr_3 , Cr_6 - As_6 - Cr_6 , Cr_2 - As_2 - Cr_2 , and Cr_5 - As_5 - Cr_5 . In the following, we study the magnetic phases and the way they get correlated to structural deformations parametrized by the in-plane angles between the Cr atoms in the isosceles triangles and the different Cr-As-Cr bonding angles. The analysis is performed as a function of the Coulomb repulsion U , for different choices of the chemical substitution.

A. Chain ground state of $Cs_2Cr_3As_3$

We apply the procedure already presented in Ref. [34] for the $K_2Cr_3As_3$ to the representative case of the $Cs_2Cr_3As_3$, and perform the atomic relaxation at different values of the Coulomb repulsion U for the distorted triangles composed of Cr atoms and belonging to the DWSN. We consider four possible collinear magnetic states, which for moderate values of U turn out to be the magnetic stable states. They are reported in Fig. 2 and are classified as the ferromagnetic state, the interlayer antiferromagnetic state, the up-up-down/up-up-down stripe state ($\uparrow\uparrow\downarrow - \uparrow\uparrow\downarrow$) and the up-up-down/down-down-up zigzag state ($\uparrow\uparrow\downarrow - \downarrow\downarrow\uparrow$). Together with these states, we also consider the nonmagnetic (NM) one.

In Fig. 3 the energy difference between the NM, FM, AFM, and the zigzag states with respect to the stripe state ($\uparrow\uparrow\downarrow - \uparrow\uparrow\downarrow$) displays the existence of two regimes: for values

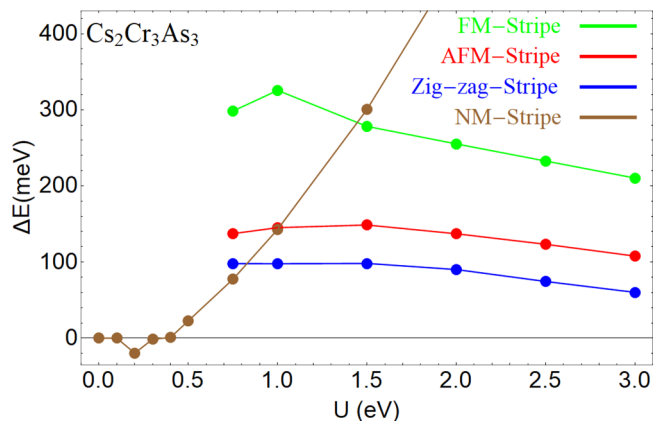


FIG. 3. Energies per Cr atom of the FM, AFM, zigzag, and NM states measured with respect to the stripe state energy, plotted as functions of the Coulomb repulsion for the compound $\text{Cs}_2\text{Cr}_3\text{As}_3$.

of the Coulomb repulsion $U < U_c = 0.4$ eV, the ground state is nonmagnetic, then becoming the stripe one for $U \geq U_c$. In the following, we will also refer to the stripe ground state as ferrimagnetic, standing for a collinear configuration where the magnetic moments are uncompensated within the unit cell, and the resulting moment is due to the majority spins of the Cr ions at the basis of each triangle.

In Figs. 4 and 5 we report the behavior of the representative angle α_1 shown in Fig. 1 and the magnetic moment m_1 at the Cr_1 site as functions of U . The other angles and magnetic moments have a very similar trend and thus are not reported here. We can see from Fig. 4 that α_1 is always away from the ideal 60° value, even in the NM phase, the only exception being represented by the FM state. In particular, while in the magnetic phases α_1 is characterized by a nonmonotonic behavior as U is varied, on the contrary in the NM phase α_1 stays almost constant, since there is no interplay between structural and magnetic properties. In particular, we note that in the stripe phase α_1 shows a sudden jump to $\sim 70^\circ$ at $U \simeq U_c$, and becomes practically constant above $U = 1.5$ eV, differently from what happens in the other magnetic configurations.

The behavior of the magnetic moment at the Cr_1 site shown in Fig. 5 confirms the strong interplay between structural and

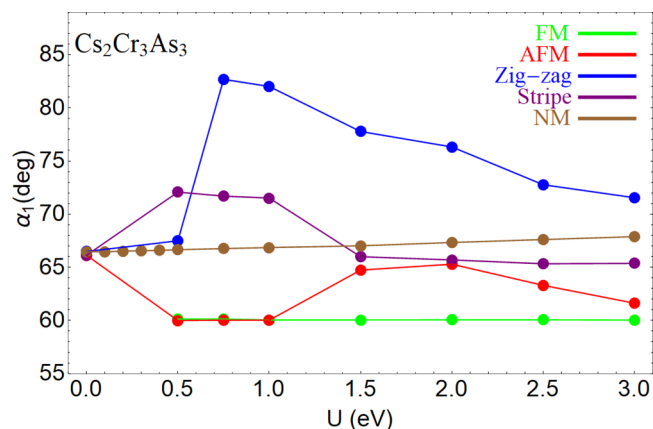


FIG. 4. Angle α_1 as a function of the Coulomb repulsion for the compound $\text{Cs}_2\text{Cr}_3\text{As}_3$.

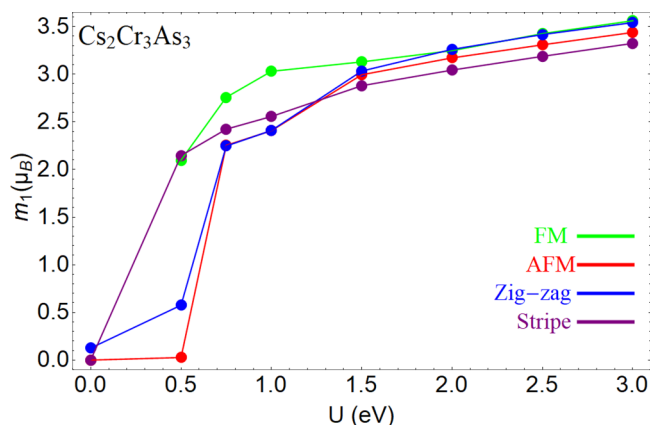


FIG. 5. Magnetic moment of the Cr_1 ion as a function of the Coulomb repulsion for the compound $\text{Cs}_2\text{Cr}_3\text{As}_3$.

spin-orbital degrees of freedom in this class of compounds. As for the case of the angle α_1 , a different behavior is found in the two regimes corresponding to values of U approximately lower and higher than 1.5 eV, respectively. At low values of U the magnetic moment tends to vanish in the zigzag as well as in the stripe phase, thus providing evidence of a nonmagnetic ground state configuration.

B. Chain ground state for different cations

In this section we report a systematic comparison of the magnetic stable phases, the α angles, and the magnetic moments for all the compounds of the family, as obtained via first-principles analysis in the same range of U and by following the same procedure.

We first point out that all the compounds show a similar behavior, i.e., the existence of a critical U_c separating the NM state ($U < U_c$) from the stripe one ($U > U_c$). We choose to focus on the most relevant comparative outcome and postpone to Appendix A the detailed results.

Figure 6 shows that chemical pressure slightly affects the U dependence of the energy difference between the zigzag and the ground stripe phase, which only shows a little re-

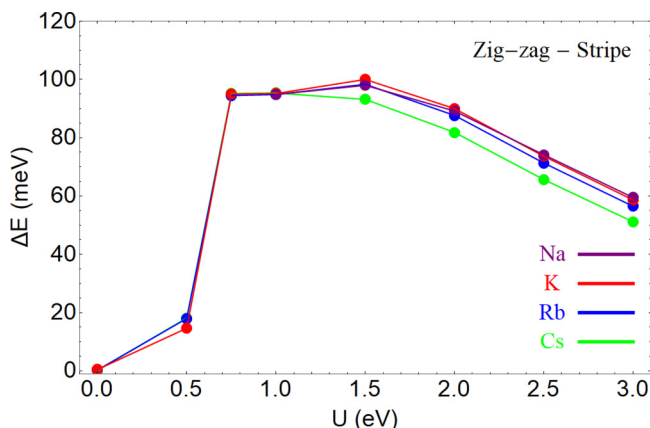


FIG. 6. Difference between the energies per Cr atom of the zigzag and of the stripe state as a function of the Coulomb interaction for the compounds of the family $\text{A}_2\text{Cr}_3\text{As}_3$ ($\text{A}=\text{Na}, \text{K}, \text{Rb}, \text{and Cs}$).

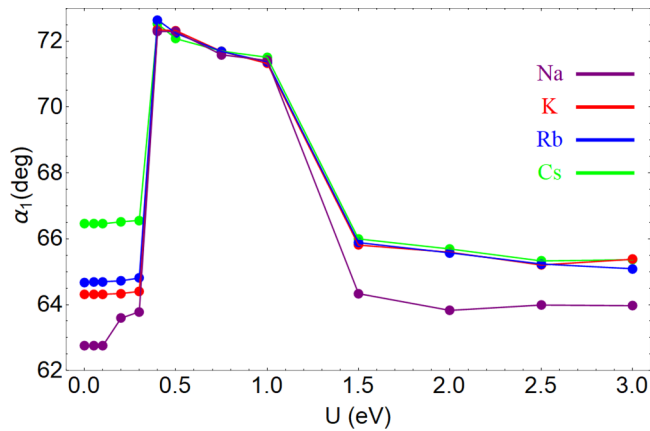


FIG. 7. Angle α_1 in the ground state as a function of the Coulomb repulsion for the compounds of the family $A_2Cr_3As_3$ ($A=Na, K, Rb,$ and Cs).

duction as the atomic radius increases. In Figs. 7 and 8 we report the comparison of the angles and the magnetic moments in the ground state for the different atomic species. We see that the Cr triangles are quite distorted in the ground phase, especially at low and intermediate values of U , this being a common trend for all the compounds. The distortion is slightly less pronounced only in the case of Na for $U > 1.5$ eV. The magnetic moment tends to grow with the ion size, saturating for larger values of U to a value that is very close to the maximum predicted value for Cr ions in the $K_2Cr_3As_3$ compound, which is $\frac{10}{3} \approx 3.33\mu_B$. This is so because the oxidation of chromium is $+2/3$ in $K_2Cr_3As_3$.

We point out that such collinear ferrimagnetic phase may be qualitatively interpreted [34] within a minimal effective Heisenberg model which assumes the Cr spins lying in the \mathbf{R}_1 - \mathbf{R}_2 plane coupled via dominant independent AFM exchange between nearest-neighbor Cr atoms and smaller AFM coupling between next-nearest-neighbor Cr atoms along the \mathbf{R}_3 axis. Specifically, the onset of the stripe phase is governed by the ratio among the in-plane exchange parameters along the

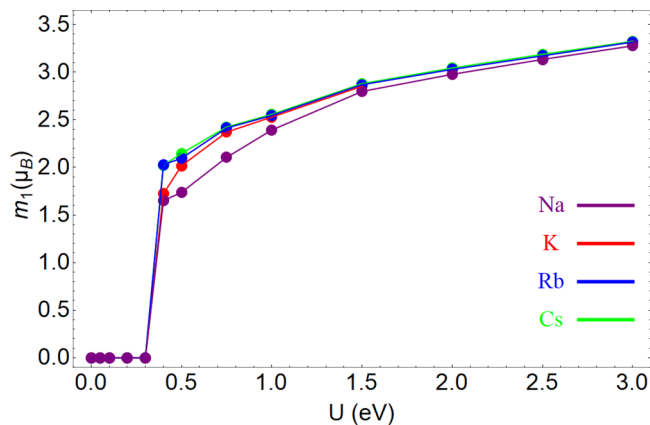


FIG. 8. Magnetic moment m_1 in the ground state as a function of the Coulomb repulsion for the compounds of the family $A_2Cr_3As_3$ ($A=Na, K, Rb,$ and Cs).

\mathbf{R}_1 and \mathbf{R}_2 axes, which in turn is critically linked to the degree of deformation of the triangles, growing with the α angles.

IV. STRENGTH OF THE MAGNETISM AND INTERCHAIN FM INSTABILITY IN THE $A_2Cr_3As_3$ FAMILY

To understand the effect of the chemical pressure due to alkali-atom substitution on the most favorable magnetic configuration in these quasi-one-dimensional systems, it is important to consider the coupling between the chains [44], which can provide useful insights for the interpretation of the experimental data [15,29,30]. In the previous section, we have shown that all the compounds have collinear magnetism above a characteristic value of U_c , where the ground state changes from a nonmagnetic to a collinear stripe configuration within the DWSN, allowing one to attribute a net magnetic moment to each chain. Single interchain magnetic interactions then couple spins of neighboring chains. Without interchain magnetic coupling, the system can only show magnetic order in one dimension, this being difficult to achieve because of the Mermin-Wagner theorem [45,46]. With the presence of the interchain magnetic coupling, the system is not one-dimensional anymore and a magnetic order can more easily develop. This crucial interchain magnetic coupling can be FM or AFM.

We study a supercell of two chains, assuming that in the magnetic phase the coupling within a single chain leads to the stripe configuration and that a macrospin can be associated to each chain.

As a first step, we proceed by looking at the energy difference between the NM, FM, and AFM interchain configurations. The study (not reported here for brevity) confirms that up to a critical value of the Coulomb repulsion the NM configuration is the ground state, and that the results for different cations are quite similar. The FM interchain configuration, where the macrospins of the chains are oriented in the same direction, is always lower in energy than the AFM one, confirming that all these compounds in this region are nonmagnetic but on the verge of magnetism, sustaining interchain FM spin fluctuations.

As a next step, we have evaluated the difference in energy of the NM state with respect to the FM one for different choices of the cation. We have performed the calculation for $U = 0.75$ eV, which guarantees an intrachain magnetism. In Fig. 9 we show that the stability of the interchain ferromagnetic coupling follows a nonmonotonic trend with increasing the ion size. Actually it grows from Na to Rb, where it assumes the maximum value, and then decreases for the Cs case. In order to explore the correlation between this trend and the features of the crystal structure, we have also evaluated the evolution of the bonding angles Cr-As-Cr upon alkali-atom substitution. In Fig. 10 we show that two of the four different bonding angles, that is, the $Cr_3-As_3-Cr_3$ and $Cr_6-As_6-Cr_6$ angles, display an evolution as a function of the ion substitution that follows the same trend (to make this more explicit, the behavior of the angle $Cr_6-As_6-Cr_6$ has been plotted in Fig. 9 together with the NM-FM energy difference). We thus deduce that the increase of these two angles may favor the interchain ferromagnetic coupling.

We can conclude that the cation substitution acts to modify the interchain structure, thus affecting the stability of

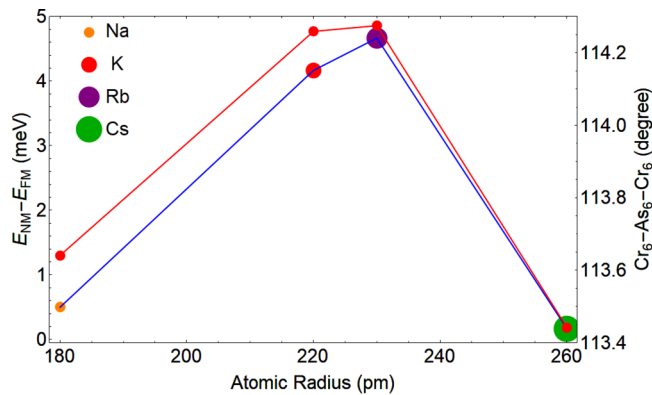


FIG. 9. Energy difference between the NM and the interchain FM state (blue line, left axis) and bonding angle $Cr_6-As_6-Cr_6$ (red line, right axis) for different choices of the cation. The value of the Coulomb repulsion is $U = 0.75$ eV.

ferromagnetism among the chains; this turns out to be favored in the Rb-based compound, while it is indeed hindered in the Cs case. We notice that recent NMR measurements suggested that $Rb_2Cr_3As_3$ may be indeed very close to a FM quantum critical point [29], while no evidence of enhancement of FM fluctuations is actually seen in the case of $Cs_2Cr_3As_3$ [30]. The mechanism which relates the structural deformation associated to the bonding angles to interchain ferromagnetism deserves further investigation.

V. STRAIN TO INDUCE MAGNETISM IN $K_2Cr_3As_3$

In this section we show that it is possible to tune the system from NM to interchain FM ground states by applying a compressive strain along a specific in-plane direction. Since the magnetic properties of these compounds are very sensitive to the modification of the total volume, we will analyze the interplay between structural and magnetic degrees of freedom in the case of fixed volume, as already explained in Sec. II.

We choose to focus on the reference case of $K_2Cr_3As_3$ and explicitly compare it with KCr_3As_3 sharing with $K_2Cr_3As_3$ quasi-one-dimensional structural features. However, in the

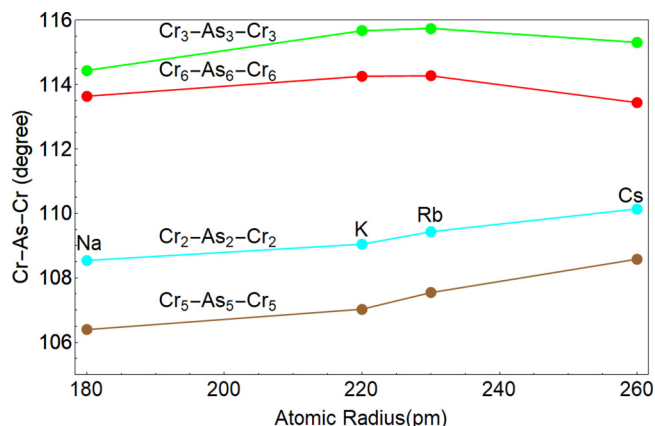


FIG. 10. Behavior of the four bonding angles $Cr-As-Cr$ for different choices of the cation. The value of the Coulomb repulsion is $U = 0.75$ eV.

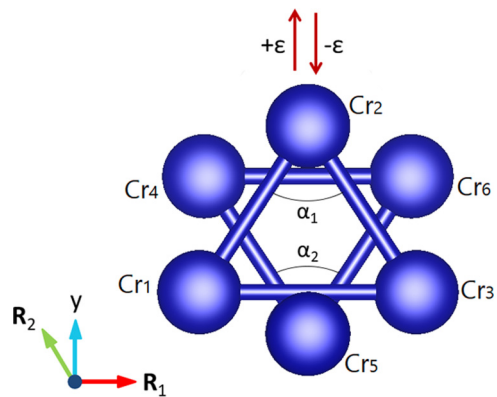


FIG. 11. Graphic representation of the strain ϵ applied orthogonally to the basis of the isosceles triangles in the chain. A negative value of ϵ indicates a compressive strain of the y component of the \mathbf{R}_2 vector, while a positive value indicates a tensile strain of the y component of the \mathbf{R}_2 vector.

latter no superconductivity was found while a spin-glasslike transition at $T_N = 5$ K was revealed by magnetic susceptibility measurements [47]. This value is very close to the superconducting critical temperature of $K_2Cr_3As_3$, indicating that the energy scales involved in the formation of the two phases are indeed comparable and that magnetism may be detrimental to the development of the superconducting phase. We also mention that KCr_3As_3 also presents a superconducting phase [48,49], though recently Taddei *et al.* [50] have shown that the emerging of this phase is due to the charge doping via H intercalation.

We start by referring to the lattice vectors of the undistorted unit cell $\mathbf{R}_1 = (a, 0, 0)$, $\mathbf{R}_2 = (-a/2, \sqrt{3}a/2, 0)$, and $\mathbf{R}_3 = (0, 0, c)$. The strain field ϵ applied to the unit cell is defined as the continuous deformation of the in-plane lattice vectors \mathbf{R}_1 and \mathbf{R}_2 . A negative value of ϵ corresponds to a compressive strain of the y component of the \mathbf{R}_2 vector, while a positive value corresponds to a tensile one. Since the volume is fixed to the value $\frac{\sqrt{3}ca^2}{2}$, the lattice vectors then become

$$\begin{aligned}\mathbf{R}_1 &= \left(\frac{a}{1+\epsilon}, 0, 0 \right), \\ \mathbf{R}_2 &= \left(-\frac{a}{2}, \frac{\sqrt{3}a(1+\epsilon)}{2}, 0 \right), \\ \mathbf{R}_3 &= (0, 0, c),\end{aligned}$$

where ϵ is dimensional and defined as $\epsilon = \Delta a/a$. The effect of this compressive (tensile) strain of the y component of the \mathbf{R}_2 vector enhances (decreases) the apex α angles as shown in Fig. 11. Due to the strong interplay between structural and magnetic degrees of freedom in this class of materials, this kind of strain is expected to have significant effects on the magnetic properties. The modules of the lattice vectors of $K_2Cr_3As_3$ for different values of the strain ϵ are reported in Table II. A similar system, namely, $K_2Mo_3As_3$, has very recently studied under pressure [51] and a modification of up to 10% of the lattice parameter a has been applied. The values of the strain that we have chosen in our analysis, i.e., $\epsilon = \pm 0.03$ and ± 0.06 , correspond to deformations of the 3%

TABLE II. Modules of the lattice vectors of $\text{K}_2\text{Cr}_3\text{As}_3$ when the strain is applied.

K_2 with strain ε	$\varepsilon = -0.06$	$\varepsilon = -0.03$	$\varepsilon = +0.03$	$\varepsilon = +0.06$
$ \mathbf{R}_1 $ (Å)	10.6204	10.2920	9.6924	9.4181
$ \mathbf{R}_2 $ (Å)	9.5375	9.7594	10.2086	10.4357
$ \mathbf{R}_3 $ (Å)	4.2304	4.2304	4.2304	4.2304

and 6% of the lattice vectors, and thus are fully in the range of an experimentally applicable strain.

The comparative analysis of the most favorable magnetic configurations within the chain for negative/positive strain demonstrates that the ground state is still NM below a critical U_c , and that above this threshold value a stripe phase is favored (see Fig. 12). Compared with the unstrained case, this value is lowered to ~ 0.3 eV when a 3% negative strain is considered, and a further slight reduction is observed when ε is further increased.

In order to provide a systematic comparison of the modifications to the ground-state magnetic and structural properties induced by a compressive/tensile strain, we report in Figs. 13 and 14 the evolution with U of the magnetic moment at the representative Cr_1 site and of the angle α_1 in the ground state, together with the analogous results recently obtained for KCr_3As_3 [34].

From the inspection of Fig. 13, we notice that the compressive and the tensile strain both allow one to tune the transition from a nonmagnetic phase with vanishing moment to a magnetic one with $m_1 \neq 0$ (turning out to be the stripe phase), but following an opposite trend. Tensile strain raises the value of U at which a finite moment appears, whereas a compressive strain tends to reduce it. In particular, for $\varepsilon = -0.06$ this value is close to the critical one marking the transition to the stripe state in KCr_3As_3 . In this context, it is significant that the angle α_1 shows an increase at the transition, particularly sharp for compressive strain, as one can see from Fig. 14.

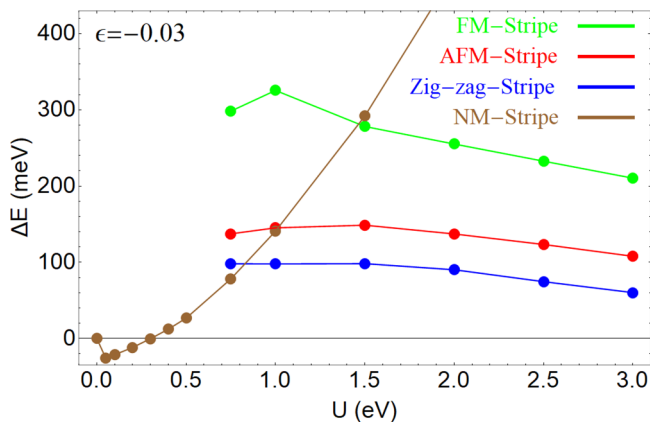


FIG. 12. Energies per Cr atom of the FM, AFM, zigzag, and NM states measured with respect to the stripe state energy, plotted as functions of the Coulomb repulsion for the compound $\text{K}_2\text{Cr}_3\text{As}_3$. A compressive strain $\varepsilon = -0.03$ is applied to the system. At low values of U some data are missing due to the lack of convergence of the numerical procedure in that regime.

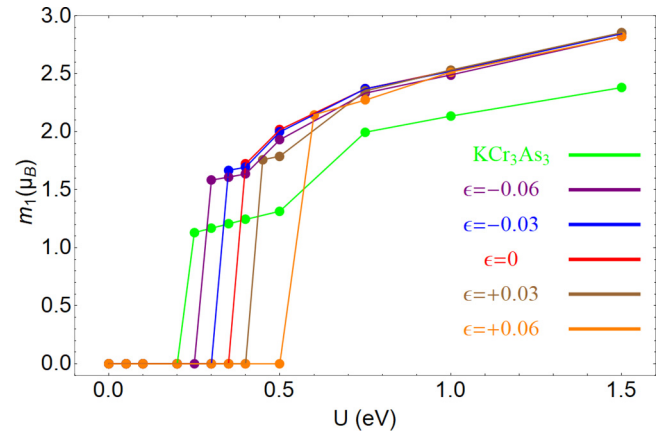


FIG. 13. Comparison of the magnetic moments of the Cr_1 atom in the ground state for different choices of compressive/tensile strain applied to $\text{K}_2\text{Cr}_3\text{As}_3$.

Next we turn to the analysis of the lowest energy configurations when the coupling between magnetic chains is considered. The collinear configurations is assumed within the chains and the calculations are performed within the PBEsol approximation. The energies of the NM, FM, and AFM configurations for $\text{K}_2\text{Cr}_3\text{As}_3$ are reported in Table III for different values of the strain. We have fixed for the Coulomb repulsion the value $U = 0.3$ eV, for which KCr_3As_3 is predicted to be magnetic, while $\text{K}_2\text{Cr}_3\text{As}_3$ is not [34]. The analysis of the interchain interactions in $\text{K}_2\text{Cr}_3\text{As}_3$ confirms the trend emerging from the study of magnetism inside the single chain. Namely, a compressive strain leads the system towards a magnetic phase, while a tensile strain stabilizes the nonmagnetic ground state. A value $\varepsilon = -0.06$ favors $\text{K}_2\text{Cr}_3\text{As}_3$ to be magnetic at $U = 0.3$ eV. The ground state is the interchain FM configuration, with the macrospins of the chains oriented in the same direction.

Hence, our results seem to indicate that the instability towards a ferrimagnetic phase can be tuned by the application of a compressive strain. This could provide important insights on the interplay between superconductivity and magnetism, possibly providing support to the idea that the

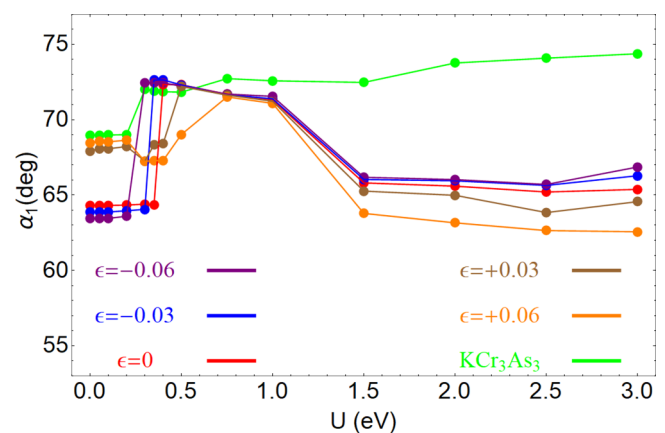


FIG. 14. Comparison of the α_1 angle in the ground state for different choices of compressive/tensile strain applied to $\text{K}_2\text{Cr}_3\text{As}_3$.

TABLE III. Energy differences (meV) of $K_2Cr_3As_3$ for NM, FM, and AFM coupling between the chains and different values of the strain. Inside the chain the stripe configuration is assumed to be the ground and the value of the Coulomb interaction is fixed at $U = 0.3$ eV.

	$\epsilon = -0.06$	$\epsilon = -0.03$	$\epsilon = 0$	$\epsilon = +0.03$	$\epsilon = +0.06$
NM	5.33	0	0	0	0
FM	0	0.25	6.92	15.25	26.75
AFM	3.92	4.08	10.83	19.75	32.00

superconducting phase arises from the suppression of the magnetic order, as controlled by the strain as a tunable parameter.

VI. ELECTRONIC PROPERTIES

In this section we analyze the electronic properties of the $A_2Cr_3As_3$ ($A=Na, K, Rb,$ and Cs) compounds in the distorted case, as well as the modifications of the electronic structure of $K_2Cr_3As_3$ under the action of a compressive or a tensile strain. We fix for the Coulomb repulsion the value $U = 0.3$ eV, for which the experimental results are satisfactorily reproduced [34].

In Figs. 15–18 we report the band structures and the orbitally resolved partial densities of states (DOSs) for the d orbitals of $A_2Cr_3As_3$ near the Fermi level. Indeed, the d orbitals have the greatest weight at the Fermi level, as in the case of the undistorted structure. We consider the partial densities of states for the d_{xy} , $d_{x^2-y^2}$, and d_{z^2} orbitals and for the d_{yz} and d_{xz} ones, which are symmetric and antisymmetric with respect to the basal plane, respectively. We make this distinction because we know from the undistorted case [12,14] that

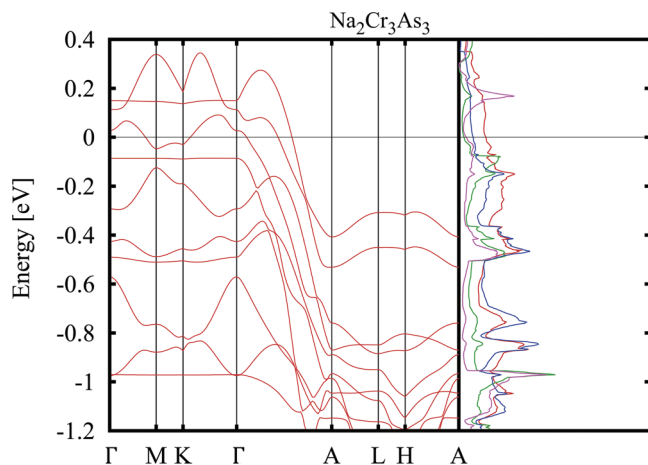


FIG. 15. Band structure of $Na_2Cr_3As_3$ near the Fermi level for $U = 0.3$ eV (left), together with the corresponding orbitally resolved partial densities of states (right). Red and green lines refer to the Cr_1 atom at the basis of the triangle and denote the DOSs projected onto orbitals symmetric with respect to the basal plane d_{xy} , $d_{x^2-y^2}$, and d_{z^2} and onto orbitals antisymmetric with respect to the basal plane d_{yz} and d_{xz} , respectively. Blue and purple lines refer to the Cr_2 atom at the vertex of the triangle and denote the DOSs projected onto the symmetric and antisymmetric orbitals, respectively.

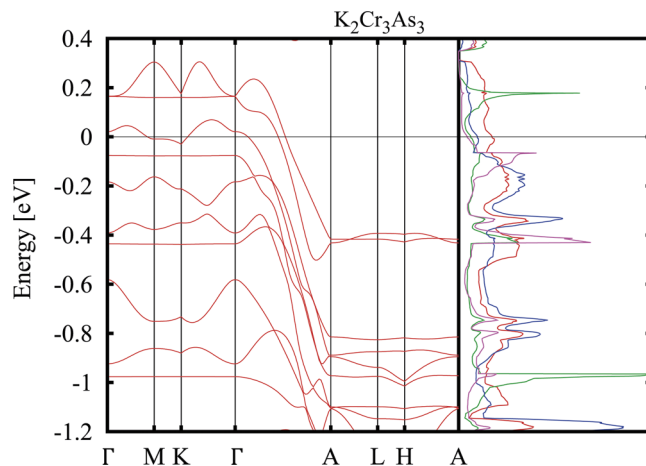


FIG. 16. Same as in Fig. 15 for $K_2Cr_3As_3$.

symmetric orbitals have a greater spectral weight at the Fermi level, while the antisymmetric ones have a relevant weight few eV far from the Fermi level. We also note that the hybridizations between the orbitals at different planes is larger than in the undistorted case because in the distorted configuration the atoms at adjacent planes are closer to each other. In the cases of Na and K the bands that cross the Fermi level (FL) are three: two of them cross the FL only along the Γ -A line, giving rise to two 1D Fermi surfaces (FSs), while the third one crosses the FL also in the plane producing a 3D FS, as in the undistorted $K_2Cr_3As_3$ material [12]. In the case of the Rb-based compound, the bands cross the FL only along the Γ -A line and the system will present three 1D FSs, while for Cs-based material we have two 1D FSs and one electron pocket, since the bands cross the FL in the plane only in few points. The Coulomb repulsion barely affects the band structure, as shown in Ref. [14], so that we can safely say that the band structure obtained for the chosen value of the Coulomb repulsion would look similar to the band structure at vanishing U . Finally, we stress that these materials can be considered as moderately correlated compounds, since a very good agreement between the DFT results, at small U , and angle-resolved photoemission spectroscopy measurements has been reported [11].

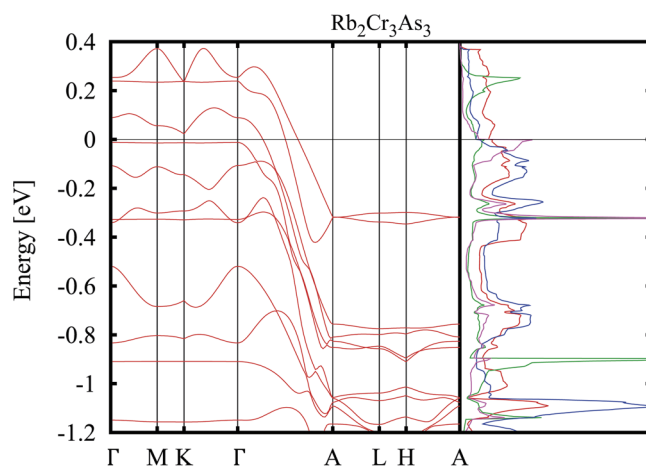
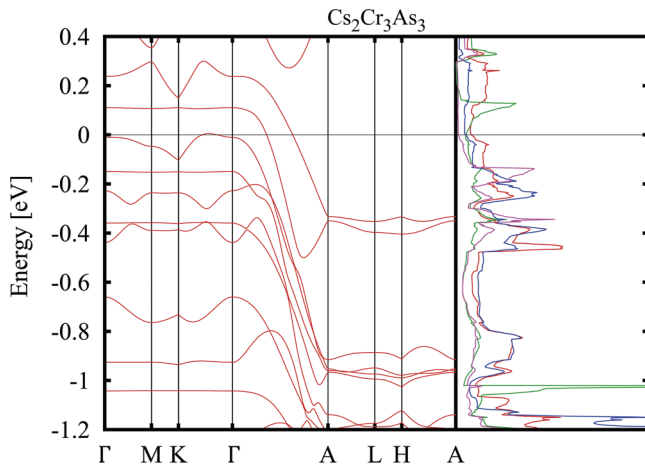


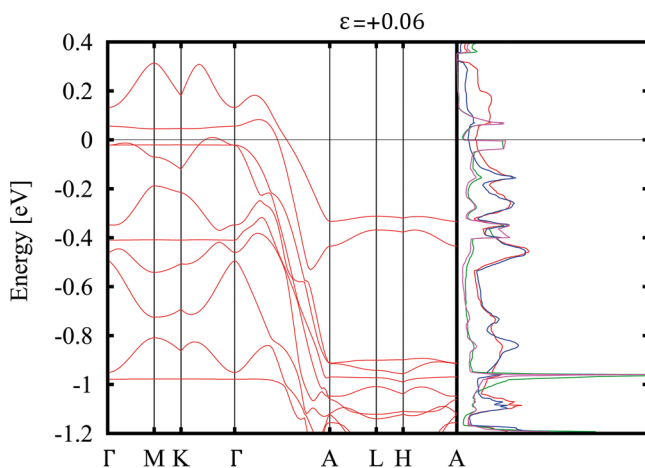
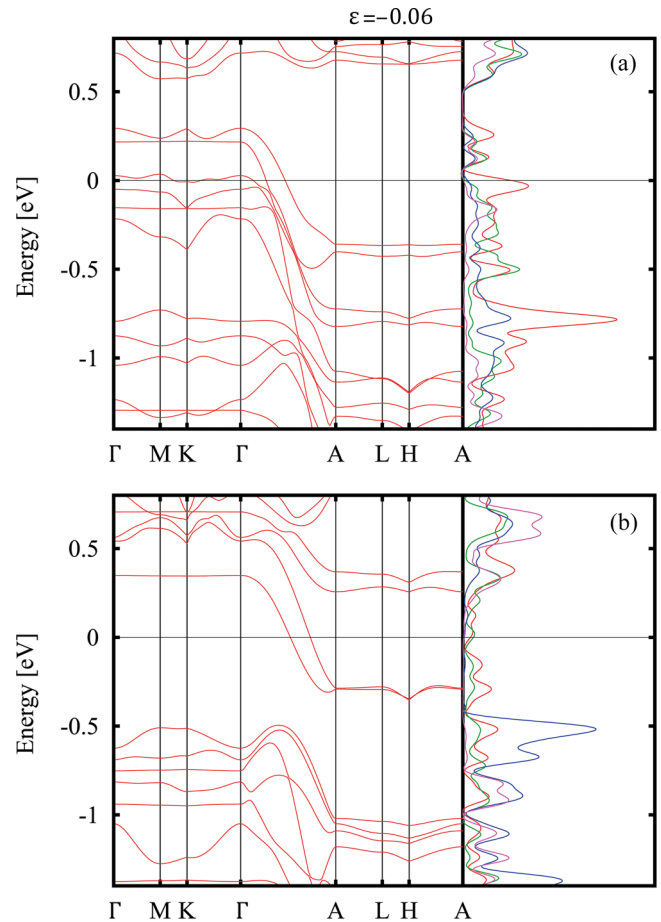
FIG. 17. Same as in Fig. 15 for $Rb_2Cr_3As_3$.

FIG. 18. Same as in Fig. 15 for $\text{Cs}_2\text{Cr}_3\text{As}_3$.

In Figs. 19 and 20 we show the band structures and the densities of states of $\text{K}_2\text{Cr}_3\text{As}_3$ under a uniaxial strain equal to $\varepsilon = \pm 0.06$. We observe that under the effects of a tensile strain, i.e., for $\varepsilon = +0.06$, the system has a nonmagnetic ground state, while in the case of a compressive strain, i.e., for $\varepsilon = -0.06$, at $U = 0.3$ eV the ground state is magnetic, as previously shown. For this reason, we report in the two panels of Fig. 20 the results concerning the spin-up and the spin-down channels. We can see from these figures that the strain modifies the number of bands that cross the FL, and hence the FS, in this way affecting the electronic properties of the system. Specifically, for $\varepsilon = +0.06$ there are two 1D FSs and one electron pocket, while for $\varepsilon = -0.06$ we can observe two 1D FSs and one 3D FS.

VII. CONCLUSIONS

We analyzed the ground state of the series $A_2\text{Cr}_3\text{As}_3$ ($A = \text{Na}, \text{K}, \text{Rb}, \text{and Cs}$) and predicted a collinear stripe configuration within the DWSN, which allows one to attribute a net magnetic moment to each chain. Due to interchain ferromagnetic coupling, all the compounds are close to a ferrimagnetic

FIG. 19. Same as in Fig. 15 for $\text{K}_2\text{Cr}_3\text{As}_3$ when a tensile strain $\varepsilon = +0.06$ is applied to the system.FIG. 20. Same as in Fig. 15 for $\text{K}_2\text{Cr}_3\text{As}_3$ when a compressive strain $\varepsilon = -0.06$ is applied to the system. In panel (a) we show the spin-up channel, while panel (b) shows the spin-down channel.

phase in the region of moderate values of the Coulomb repulsion U . The occurrence of such collinear magnetic state has an important interplay with the distortion of the triangles which reduces the frustration of the antiferromagnetic couplings between the nearest-neighbor Cr atoms.

Such behavior has been proved to be robust against the variation of the chemical pressure induced by the change of the cation among the different members of the family. Notably, we have shown that the strength of the interchain ferromagnetic coupling has a nonmonotonic behavior as a function of the atomic radius of the alkali metals. In particular, the stability of the interchain ferromagnetic coupling is gradually increased when changing from Na to Rb, while it is reduced for the Cs compound, in agreement with recent experimental observations [29,30]. We relate this behavior to the Cr-As-Cr bonding angles along the chain, this being a key factor controlling the tendency towards the interchain ferromagnetism.

As far as strain is concerned, we demonstrated that uniaxial compressive strain applied orthogonally to the basis of the isosceles triangles tends to increase the apex angles. Confirming the strong interplay between structural properties and magnetism in the above-mentioned compounds, strain has been shown to significantly affect the transition from the NM

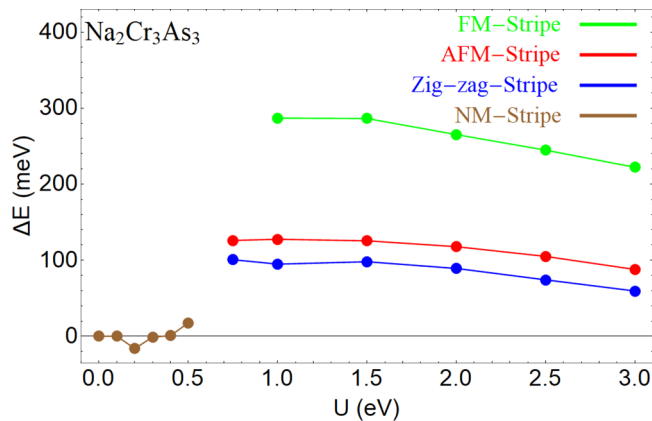


FIG. 21. Energies per Cr atom of the FM, AFM, zigzag, and NM states measured with respect to the stripe state energy, plotted as functions of the Coulomb repulsion for the compound $\text{Na}_2\text{Cr}_3\text{As}_3$. At low values of U some data are missing due to the lack of convergence of the numerical procedure in that regime.

to the ferrimagnetic phase in the regime of moderate electron correlations.

In conclusion, our results clearly show that the compounds of the family $A_2\text{Cr}_3\text{As}_3$ ($A=\text{Na}, \text{K}, \text{Rb},$ and Cs) are close to an interchain FM instability, which is significantly affected by structural effects. Our analysis can thus prove to be relevant in the study of the interplay between magnetism and superconductivity [52] experimentally detected in this class of compounds [43,53].

ACKNOWLEDGMENTS

The authors acknowledge A. Galluzzi and M. Polichetti for useful discussions. The work is supported by the Foundation for Polish Science through the International Research Agendas program cofinanced by the European Union within the Smart Growth Operational Programme. G.C. acknowledges financial support from “Fondazione Angelo Della Riccia.” X.M. was sponsored by the National Natural Science Foundation of China (Grant No. 11864008). We acknowledge the access to the computing facilities of the Interdisciplinary Center of Modeling at the University of Warsaw, Grants No. G73-23 and No. G75-10. We acknowledge the CINECA award under the ISCRA initiatives IsC69 “MAINTOP,” IsC76 “MEPBI,” and IsC81 “DISTANCE” grant for the availability of high-performance computing resources and support.

APPENDIX A: RESULTS FOR $\text{Na}_2\text{Cr}_3\text{As}_3$ AND $\text{Rb}_2\text{Cr}_3\text{As}_3$

Here we report the results concerning the energies, the angle α_1 , and the magnetic moment m_1 for the other compounds of the family $A_2\text{Cr}_3\text{As}_3$.

The energies of the various configurations investigated, measured with respect to the one of the stripe state, are plotted as functions of the Coulomb repulsion U in Figs. 21 and 22 for $\text{Na}_2\text{Cr}_3\text{As}_3$ and $\text{Rb}_2\text{Cr}_3\text{As}_3$, respectively. The case of the $\text{K}_2\text{Cr}_3\text{As}_3$ is instead reported in Ref. [34].

Our results show a similar behavior for the two compounds, this indicating that the chemical pressure due to the

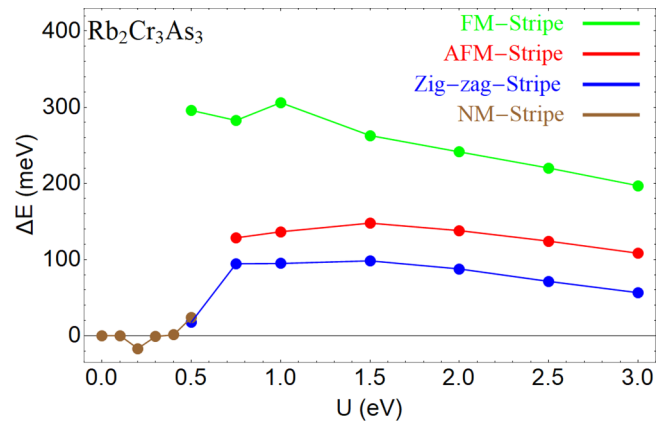


FIG. 22. Same as in Fig. 21 for the compound $\text{Rb}_2\text{Cr}_3\text{As}_3$.

change of the cation alters only slightly the nature of the magnetic configuration within the chain. For all the compounds the ground state is nonmagnetic for values of the Coulomb repulsion $U < U_c = 0.4$ eV, then becoming the stripe one for $U \geq U_c$. On the other hand, the energy in the ferromagnetic configuration is always larger than in the other phases, this situation remaining the same for all the compounds.

The angle α_1 as a function of U is plotted in Figs. 23 and 24 for Na and Rb cations, respectively. The various configurations always correspond to distorted triangles, except for the fully FM one, and, in the case of $\text{Na}_2\text{Cr}_3\text{As}_3$, also for the AFM one. For all the compounds, the increase of U above a value approximately equal to 1.5 eV does not produce significant variations of α_1 , the only exception being the zigzag configuration for which α_1 decreases appreciably as U is increased. The magnetic moment of the Cr_1 ion is reported for the two cases $A=\text{Na}, \text{Rb}$ in Figs. 25 and 26, respectively. For $U > 1.5$ eV it approaches the maximum predicted value for Cr ions in $A_2\text{Cr}_3\text{As}_3$, which is $10/3\mu_B$. On the other hand, for small values of the Coulomb repulsion the magnetic moment tends to vanish, in agreement with the fact that the ground state in this regime is nonmagnetic.

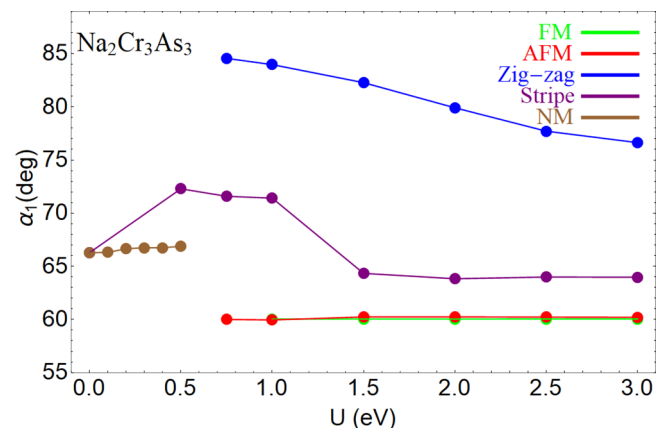
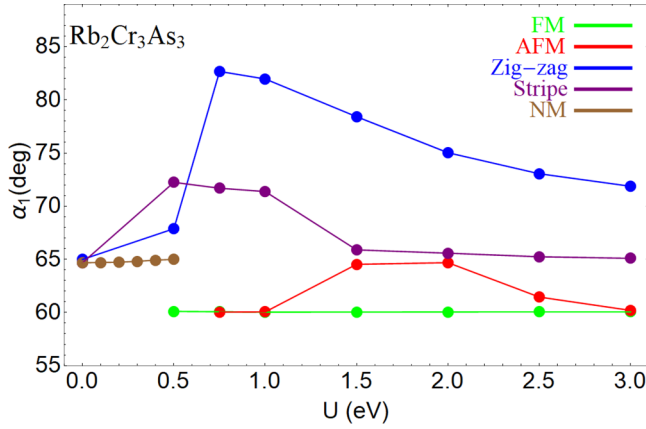


FIG. 23. Angle α_1 as a function of the Coulomb repulsion for the compound $\text{Na}_2\text{Cr}_3\text{As}_3$. At low values of U some data are missing due to the lack of convergence of the numerical procedure in that regime.

FIG. 24. Same as in Fig. 23 for the compound $\text{Rb}_2\text{Cr}_3\text{As}_3$.

APPENDIX B: MAGNETIC EXCHANGES

In this Appendix, we map the DFT results into the Heisenberg model, providing an estimation of the exchange couplings and explaining the limitations of the method when applied to the class of materials under consideration. First we provide the results for the magnetic exchanges in $\text{A}_2\text{Cr}_3\text{As}_3$ ($\text{A}=\text{Na}, \text{K}, \text{Rb}, \text{and Cs}$) as functions of U , then we plot their evolution as a function of the strain for $\text{K}_2\text{Cr}_3\text{As}_3$, as described in the main text.

The mapping of the DFT results on the Heisenberg model can be obtained calculating the energy of several magnetic configurations. The reliability of this method depends on the values of the magnetic moments that should be constant in each of the magnetic configurations. While this holds for $U \gtrsim 1.5$ eV, we have found that the magnetic moment appreciably varies for $U < 1.5$ eV. However, our results show that it is still possible to perform the mapping of the DFT results into the Heisenberg model for 0.75 eV $\lesssim U < 1.5$ eV, but for this class of materials we are on the verge of the applicability of the mapping to the Heisenberg model. Since we know that the magnetic coupling should go to zero for $U < 0.3$ eV, we extrapolate the results from $U = 0.75$ eV to $U = 0.3$ eV to

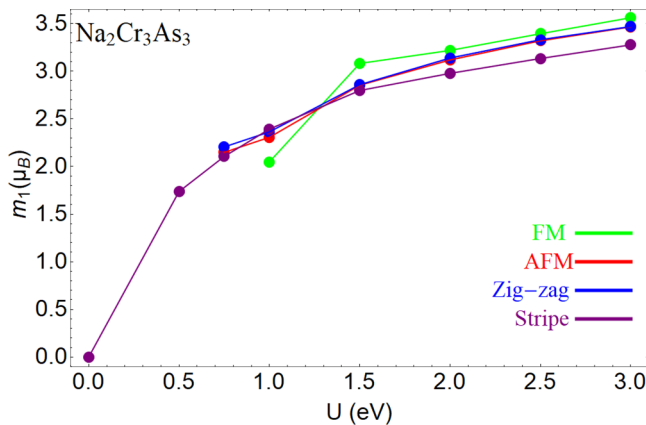
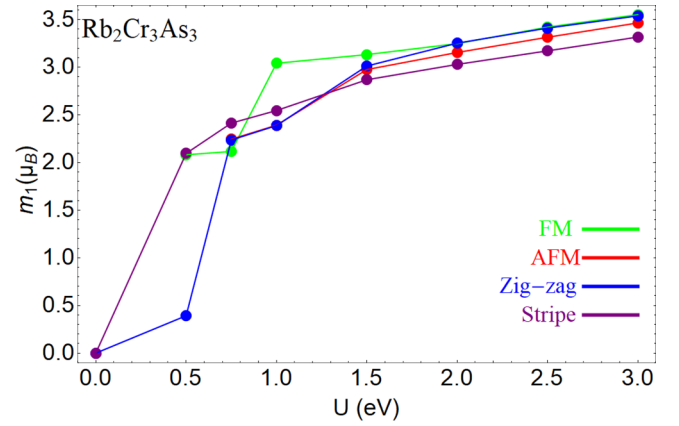


FIG. 25. Magnetic moment of the Cr_1 ion, as a function of the Coulomb repulsion for the compound $\text{Na}_2\text{Cr}_3\text{As}_3$. At low values of U some data are missing due to the lack of convergence of the numerical procedure in that regime.

FIG. 26. Same as in Fig. 25 for the compound $\text{Rb}_2\text{Cr}_3\text{As}_3$.

have an indication of the magnetic coupling in the range of U that better describes the properties of the system.

To perform the mapping and have an estimation of the nearest-neighbor magnetic coupling, we assume that the two interlayer magnetic couplings are equal and we calculate the energy for a new magnetic configuration in addition to the previous ones shown in Fig. 2 and investigated in the main text. The new magnetic configuration has the Cr atoms at the basis with opposite spin direction as shown in Fig. 27. We exclude the ferromagnetic phase configuration for the mapping because its equation is linearly dependent on the others in the linear equation system.

To evaluate the magnetic exchange couplings, we adopt the following Heisenberg Hamiltonian [34]:

$$H = \sum_{(i,j,\mu \leq \nu)} J_{i,j}^{\mu,\nu} S_i^\mu S_j^\nu. \quad (\text{B1})$$

Here the sum is over pairs of adjacent spins in the $z = 0$ and/or $z = 0.5$ planes, and $\mu, \nu \in \{0, 1\}$. If $\mu, \nu = 0$ the spins are both in the plane located at $z = 0$, if $\mu, \nu = 1$ they both

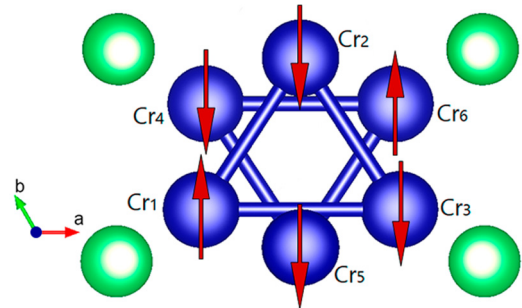


FIG. 27. Arrangements of the Cr spin of the magnetic configuration investigated in addition to the previous ones discussed in the main text in order to obtain the magnetic exchanges. This new magnetic configuration, which we name “stripe2” for further reference, has the Cr atoms at the basis with opposite spin direction. J_a is the magnetic coupling between the Cr atoms at the basis and those at the apex of the isosceles triangles, as for example, Cr_1 and Cr_2 ; J_b is the magnetic coupling between the two Cr atoms at the basis, as Cr_1 and Cr_3 . J_c is the interplane coupling constant, relating, for example, to atoms Cr_1 and Cr_4 .

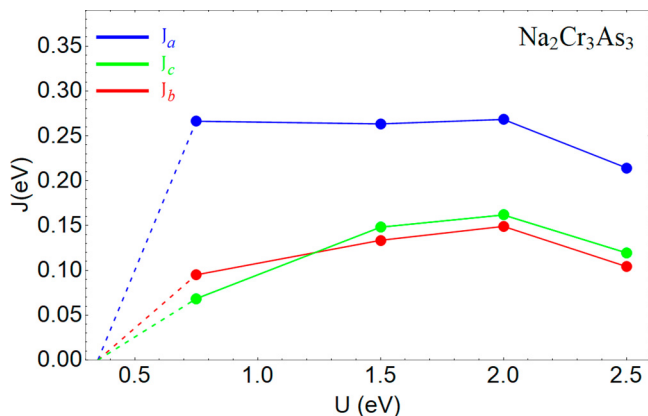


FIG. 28. Magnetic exchanges for Na₂Cr₃As₃ as functions of the Coulomb repulsion U . J_a , J_b , and J_c are three magnetic exchanges defined in the text. The dashed line indicates the extrapolation in the region where the mapping is not possible.

lie in the plane at $z = 0.5$, and if $\mu \neq \nu$ the two spins are in different planes. When the coupling is antiferromagnetic, the value of J is positive in our convention. The energies in the four configurations that we have considered are

$$E_{\text{AFM}} = S^2(2J_b + 4J_a - 12J_c) + E_0, \quad (\text{B2})$$

$$E_{\text{stripe}} = S^2(2J_b - 4J_a - 4J_c) + E_0, \quad (\text{B3})$$

$$E_{\text{zigzag}} = S^2(2J_b - 4J_a + 4J_c) + E_0, \quad (\text{B4})$$

$$E_{\text{stripe2}} = S^2(-2J_b - 4J_c) + E_0. \quad (\text{B5})$$

Here E_0 denotes the nonmagnetic ground-state energy; E_{AFM} , E_{stripe} , and E_{zigzag} are the energies of the AFM, stripe, and zigzag magnetic moment configurations shown in Figs. 2(b)–2(d), respectively; and E_{stripe2} is the energy of the configuration shown in Fig. 27. From these equations we obtained the exchange couplings. As in Ref. [34], we indicate with J_a the magnetic coupling between the Cr atoms at the basis and those at the apex of the isosceles triangles, as for

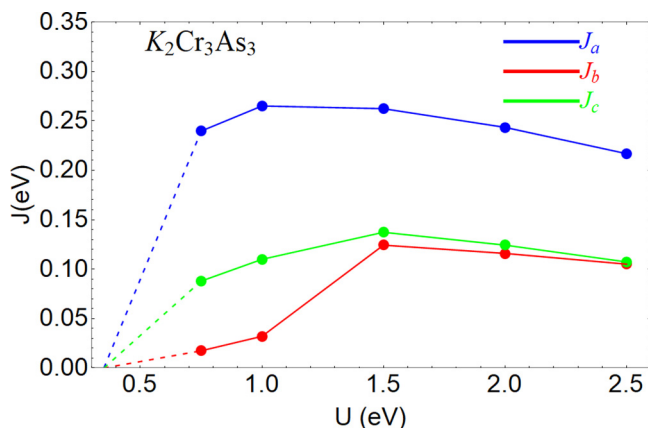


FIG. 29. Magnetic exchanges for K₂Cr₃As₃ as functions of the Coulomb repulsion U . J_a , J_b , and J_c are three magnetic exchanges defined in the text. The dashed line indicates the extrapolation in the region where the mapping is not possible.

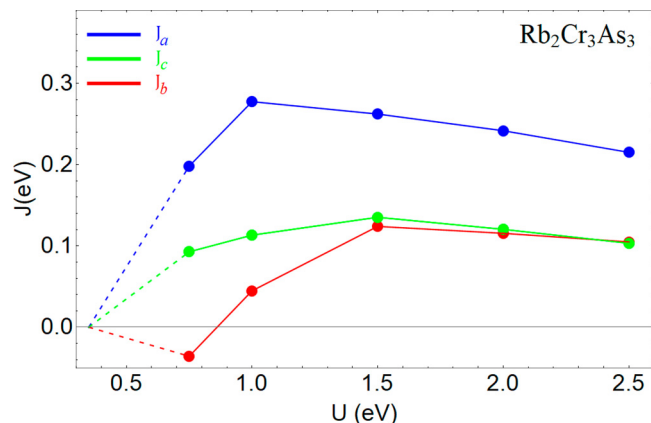


FIG. 30. Magnetic exchanges for Rb₂Cr₃As₃ as functions of the Coulomb repulsion U . J_a , J_b , and J_c are three magnetic exchanges defined in the text. The dashed line indicates the extrapolation in the region where the mapping is not possible.

example, Cr₁ and Cr₂ of Fig. 27, while J_b is the magnetic coupling between the two Cr atoms at the basis, as Cr₁ and Cr₃. J_c is the interplane coupling constant, relating, for example, to atoms Cr₁ and Cr₄. The magnetic exchanges for A₂Cr₃As₃ (A=Na, K, Rb, and Cs) as functions of U are reported in Figs. 28–31. In the case of Na and K, all the nearest-neighbor magnetic exchanges are antiferromagnetic for every value of U , including the value $U = 2$ eV that is also reported in the literature for the undistorted case [8]. The in-plane magnetic coupling J_a is larger than J_b , this stabilizing the collinear magnetic configuration, as reported in Ref. [34]. Moreover, the interlayer magnetic coupling is larger than the previously calculated magnetic couplings [8], this being presumably due to the increase of the distortions that reduces the strength of the interlayer Cr-Cr bonds. In the cases of the two heaviest cations, i.e., Rb and Cs, J_b is negative at $U = 0.75$ eV, therefore the atoms at the basis of the triangle are ferromagnetically coupled and the system is no longer frustrated. In the case of Na, the lightest cation, the points at $U = 1$ eV are missing because of the lack of convergence of the magnetic configura-

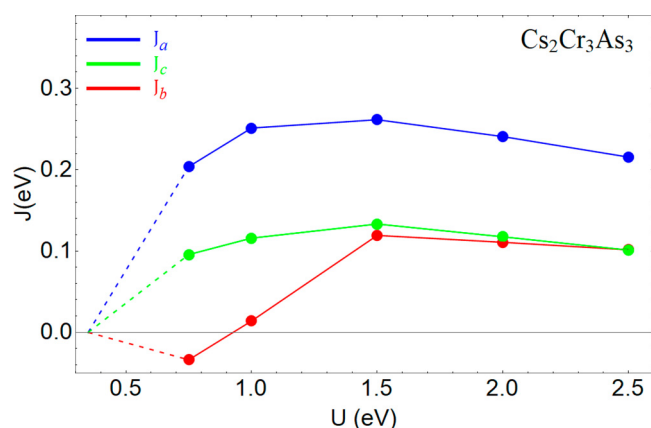


FIG. 31. Magnetic exchanges for Cs₂Cr₃As₃ as functions of the Coulomb repulsion U . J_a , J_b , and J_c are three magnetic exchanges defined in the text. The dashed line indicates the extrapolation in the region where the mapping is not possible.

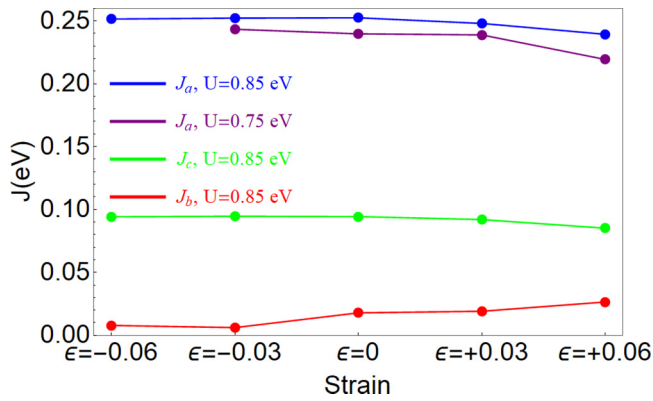


FIG. 32. Magnetic exchanges of $K_2Cr_3As_3$ as functions of the strain for $U = 0.85$ eV and J_a in the case of $U = 0.75$ eV. J_a , J_b , and J_c are three magnetic exchanges defined in the text.

tion with three parallel spins that strongly prefer to be aligned antiparallel.

In Fig. 32, we plot the magnetic exchanges as functions of the strain for $K_2Cr_3As_3$ at $U = 0.85$ eV, this being the lowest value of U where the mapping is possible for every value of the strain. While the magnetic exchanges are very sensitive to the Coulomb repulsion U , the dependence on the strain is much weaker, as expected from the other results discussed in the main text. We also report the behavior of J_a for $U = 0.75$ eV showing that the main magnetic coupling J_a increases as a function of U for every value of the strain. We see that a tensile (positive) strain brings towards a nonmagnetic phase, as stated in the main text of the paper (see Fig. 32). We cannot map the J 's for $U = 0.3$ eV, but we expect that for negative value of the strain the magnetic couplings are still sizable, in such a way that we can observe a long-range magnetic order in the presence of interchain magnetic coupling [34].

As far as the estimation of the critical temperature is concerned, since the system is quasi-one-dimensional with frustrated magnetism, a mean-field approach fails to provide a correct estimation of T_N . Rather, we should include in the calculation the effect of the interchain exchange interactions, but this is beyond the scope of the present paper.

- [1] Q.-G. Mu, B.-B. Ruan, B.-J. Pan, T. Liu, J. Yu, K. Zhao, G.-F. Chen, and Z.-A. Ren, *Phys. Rev. Mater.* **2**, 034803 (2018).
- [2] J.-K. Bao, J.-Y. Liu, C.-W. Ma, Z.-H. Meng, Z.-T. Tang, Y.-L. Sun, H.-F. Zhai, H. Jiang, H. Bai, C.-M. Feng, Z.-A. Xu, and G.-H. Cao, *Phys. Rev. X* **5**, 011013 (2015).
- [3] Z.-T. Tang, J.-K. Bao, Y. Liu, Y.-L. Sun, A. Ablimit, H.-F. Zhai, H. Jiang, C.-M. Feng, Z.-A. Xu, and G.-H. Cao, *Phys. Rev. B* **91**, 020506(R) (2015).
- [4] Z.-T. Tang, J.-K. Bao, Z. Wang, H. Bai, H. Jiang, Y. Liu, H.-F. Zhai, C.-M. Feng, Z.-A. Xu, and G.-H. Cao, *Sci. Chin. Mater.* **58**, 16 (2015).
- [5] K. M. Taddei, Q. Zheng, A. S. Sefat, and C. de la Cruz, *Phys. Rev. B* **96**, 180506(R) (2017).
- [6] K. M. Taddei, G. Xing, J. Sun, Y. Fu, Y. Li, Q. Zheng, A. S. Sefat, D. J. Singh, and C. de La Cruz, *Phys. Rev. Lett.* **121**, 187002 (2018).
- [7] C. Noce, *EPL (Europhys. Lett.)* **130**, 67001 (2020).
- [8] X.-X. Wu, C.-C. Le, J. Yuan, H. Fan, and J.-P. Hu, *Chin. Phys. Lett.* **32**, 057401 (2015).
- [9] S.-Q. Wu, C. Cao, and G.-H. Cao, *Phys. Rev. B* **100**, 155108 (2019).
- [10] T. Kong, S. L. Bud'ko, and P. C. Canfield, *Phys. Rev. B* **91**, 020507(R) (2015).
- [11] M. D. Watson, Y. Feng, C. W. Nicholson, C. Monney, J. M. Riley, H. Iwasawa, K. Refson, V. Sacksteder, D. T. Adroja, J. Zhao, and M. Hoesch, *Phys. Rev. Lett.* **118**, 097002 (2017).
- [12] H. Jiang, G. Cao, and C. Cao, *Sci. Rep.* **5**, 16054 (2015).
- [13] G. Cuono, C. Autieri, F. Forte, G. Busiello, M. T. Mercaldo, A. Romano, C. Noce, and A. Avella, *AIP Adv.* **8**, 101312 (2018).
- [14] G. Cuono, C. Autieri, F. Forte, M. T. Mercaldo, A. Romano, A. Avella, and C. Noce, *New J. Phys.* **21**, 063027 (2019).
- [15] H. Z. Zhi, T. Imai, F. L. Ning, J.-K. Bao, and G.-H. Cao, *Phys. Rev. Lett.* **114**, 147004 (2015).
- [16] D. T. Adroja, A. Bhattacharyya, M. Telling, Y. Feng, M. Smidman, B. Pan, J. Zhao, A. D. Hillier, F. L. Pratt, and A. M. Strydom, *Phys. Rev. B* **92**, 134505 (2015).
- [17] G. M. Pang, M. Smidman, W. B. Jiang, J. K. Bao, Z. F. Weng, Y. F. Wang, L. Jiao, J. L. Zhang, G. H. Cao, and H. Q. Yuan, *Phys. Rev. B* **91**, 220502(R) (2015).
- [18] W. Wu, X. Zhang, Z. Yin, P. Zheng, N. Wang, and J. Luo, *Sci. China Phys. Mech. Astron.* **53**, 1207 (2010).
- [19] W. Wu, J. Cheng, K. Matsubayashi, P. Kong, F. Lin, C. Jin, N. Wang, Y. Uwatoko, and J. Luo, *Nat. Commun.* **5**, 5508 (2014).
- [20] H. Kotegawa, S. Nakahara, H. Tou, and H. Sugawara, *J. Phys. Soc. Jpn.* **83**, 093702 (2014).
- [21] C. Autieri and C. Noce, *Philos. Mag.* **97**, 3276 (2017).
- [22] C. Autieri, G. Cuono, F. Forte, and C. Noce, *J. Phys.: Condens. Matter* **29**, 224004 (2017).
- [23] C. Autieri, G. Cuono, F. Forte, and C. Noce, *J. Phys. Conf. Ser.* **969**, 012106 (2018).
- [24] G. Cuono, C. Autieri, G. Guarnaccia, A. Avella, M. Cuoco, F. Forte, and C. Noce, *Eur. Phys. J.: Spec. Top.* **228**, 631 (2019).
- [25] G. Cuono, F. Forte, M. Cuoco, R. Islam, J. Luo, C. Noce, and C. Autieri, *Phys. Rev. Mater.* **3**, 095004 (2019).
- [26] A. Nigro, P. Marra, C. Autieri, W. Wu, J. G. Cheng, J. Luo, and C. Noce, *Europhys. Lett.* **125**, 57002 (2019).
- [27] J. Luo, J. Yang, R. Zhou, Q. G. Mu, T. Liu, Z.-A. Ren, C. J. Yi, Y. G. Shi, and G.-Q. Zheng, *Phys. Rev. Lett.* **123**, 047001 (2019).
- [28] See, for instance, G. Goll, *Unconventional Superconductors* (Springer, Berlin, 2006).
- [29] J. Yang, Z.-T. Tang, G.-H. Cao, and G.-Q. Zheng, *Phys. Rev. Lett.* **115**, 147002 (2015).
- [30] H. Zhi, D. Lee, T. Imai, Z. Tang, Y. Liu, and G. Cao, *Phys. Rev. B* **93**, 174508 (2016).
- [31] A. Subedi, *Phys. Rev. B* **92**, 174501 (2015).
- [32] H.-T. Zhong, X.-Y. Feng, H. Chen, and J.-H. Dai, *Phys. Rev. Lett.* **115**, 227001 (2015).
- [33] X. X. Wu, F. Yang, C. C. Le, H. Fan, and J. P. Hu, *Phys. Rev. B* **92**, 104511 (2015).

- [34] G. Cuono, F. Forte, A. Romano, X. Ming, J. Luo, C. Autieri, and C. Noce, *Phys. Rev. B* **103**, 214406 (2021).
- [35] G. Kresse and J. Hafner, *Phys. Rev. B* **47**, 558(R) (1993).
- [36] G. Kresse and J. Furthmüller, *Comput. Mater. Sci.* **6**, 15 (1996).
- [37] G. Kresse and J. Furthmüller, *Phys. Rev. B* **54**, 11169 (1996).
- [38] G. Kresse and D. Joubert, *Phys. Rev. B* **59**, 1758 (1999).
- [39] J. P. Perdew, A. Ruzsinszky, G. I. Csonka, O. A. Vydrov, G. E. Scuseria, L. A. Constantin, X. Zhou, and K. Burke, *Phys. Rev. Lett.* **100**, 136406 (2008).
- [40] A. I. Liechtenstein, V. I. Anisimov, and J. Zaanen, *Phys. Rev. B* **52**, R5467(R) (1995).
- [41] C. Cao, H. Jiang, X.-Y. Feng, and J. Dai, *Phys. Rev. B* **92**, 235107 (2015).
- [42] J. P. Sun, Y. Y. Jiao, C. L. Yang, W. Wu, C. J. Yi, B. S. Wang, Y. G. Shi, J. L. Luo, Y. Uwatoko, and J.-G. Cheng, *J. Phys.: Condens. Matter* **29**, 455603 (2017).
- [43] Z. Wang, W. Yi, Q. Wu, V. A. Sidorov, J. Bao, Z. Tang, J. Guo, Y. Zhou, S. Zhang, H. Li, Y. Shi, X. Wu, L. Zhang, K. Yang, A. Li, G. Cao, J. Hu, L. Sun, and Z. Zhao, *Sci. Rep.* **6**, 37878 (2016).
- [44] G. Cuono, C. Autieri, and M. M. Wysokiński, [arXiv:2104.04245](https://arxiv.org/abs/2104.04245).
- [45] A. Gelfert and W. Nolting, *J. Phys: Condens. Matter* **13**, 505 (2001).
- [46] C. Noce, *Phys. Rep.* **431**, 173 (2006).
- [47] J.-K. Bao, L. Li, Z.-T. Tang, Y. Liu, Y.-K. Li, H. Bai, C.-M. Feng, Z.-A. Xu, and G.-H. Cao, *Phys. Rev. B* **91**, 180404(R) (2015).
- [48] Q. G. Mu, B. B. Ruan, B. J. Pan, T. Liu, J. Yu, K. Zhao, G. F. Chen, and Z. A. Ren, *Phys. Rev. B* **96**, 140504(R) (2017).
- [49] T. Liu, Q. G. Mu, B. J. Pan, J. Yu, B. B. Ruan, K. Zhao, G. F. Chen, and Z. A. Ren, *Europhys. Lett.* **120**, 27006 (2018).
- [50] K. M. Taddei, L. D. Sanjeewa, B.-H. Lei, Y. Fu, Q. Zheng, D. J. Singh, A. S. Sefat, and C. dela Cruz, *Phys. Rev. B* **100**, 220503(R) (2019).
- [51] C. Huang, J. Guo, K. Zhao, F. Cui, S. Qin, Q. Mu, Y. Zhou, S. Cai, C. Yang, S. Long, K. Yang, A. Li, Q. Wu, Z. Ren, J. Hu, and L. Sun, *Phys. Rev. Mater.* **5**, L021801 (2021).
- [52] A. Galluzzi, G. Cuono, A. Romano, J. Luo, C. Autieri, C. Noce, and M. Polichetti (unpublished).
- [53] C. Xu, N. Wu, G.-X. Zhi, B.-H. Lei, X. Duan, F. Ning, C. Cao, and Q. Chen, *NPJ Comput. Mater.* **6**, 30 (2020).